Wuhan University
Journal of Natural Sciences

2021, Vol.26 No.6, 513-520

Article ID 1007-1202(2021)06-0513-08
DOI https://doi.org/10.1051/wujns/2021266513

A Design of Nonlinear Scaling and Nonlinear Optimal Motion Cueing Algorithm for Pilot's Station

☐ **ZHU Daoyang, YAN Jun, DUAN Shaoli**

College of Intelligent Manufacturing, Wuhan Technical College of Communications, Wuhan 430065, Hubei, China

Abstract: Motion cueing algorithms (MCA) are often applied in the motion simulators. In this paper, a nonlinear optimal MCA, taking into account translational and rotational motions of a simulator within its physical limitation, is designed for the motion platform aiming to minimize human's perception error in order to provide a high degree of fidelity. Indeed, the movement sensation center of most MCA is placed at the center of the upper platform, which may cause a certain error. Pilot's station should be paid full attention to in the MCA. Apart from this, the scaling and limiting module plays an important role in optimizing the motion platform workspace and reducing false cues during motion reproduction. It should be used along within the washout filter to decrease the amplitude of the translational and rotational motion signals uniformly across all frequencies through the MCA. A nonlinear scaling method is designed to accurately duplicate motions with high realistic behavior and use the platform more efficiently without violating its physical limitations. The simulation experiment is verified in the longitudinal/pitch direction for motion simulator. The result implies that the proposed method can not only overcome the problem of the workspace limitations in the simulator motion reproduction and improve the realism of movement sensation, but also reduce the false cues to improve dynamic fidelity during the motion simulation process.

Key words: nonlinear optimal motion cueing algorithm (MCA); nonlinear scaling and limiting; pilot's station; dynamic fidelity
CLC number: TP 391.9; V 211.73

Received date: 2021-09-08
Foundation item: Supported by Natural Science Foundation of Hubei Province (2019CFB693), Scientific Research Guiding Project of Education Department of Hubei Province (B2020418)
Biography: ZHU Daoyang, male, Lecturer, Master, research direction: flight simulation technology. E-mail: dyzhu_xg@aliyun.com

0 Introduction

The purpose of the washout filter is to provide the motion cues representing realistic human perception, beside the motion must proceed within the bounds of the simulator workspace. Three approaches to develop motion cueing algorithm (MCA) have been put forward, which are designed to "trick" a person into believing that driver is experiencing cues similar to those in a real flight. Conrad *et al*[1] proposed the classical MCA in the first place. The scheme has simple structure, fast execution and feedback speed[2], but it also has several shortcomings, e.g. the key one is a fixed scheme of the classical washout filters as a result of inappropriate weight-tuning of the associated parameters[3]. The adaptive MCA is the second method. Bowles *et al*[4] developed a modification of the coordinated adaptive MCA. The third method is the optimal MCA which was developed by Sivan *et al*[5] and later implemented by Reid *et al*[6]. There are two types of optimal MCA, linear and nonlinear. Note that both algorithms are designed based on the same principles and concepts. The major differences are in real-time implementation of washout filters for the solution to the Riccati equation. No matter what kind of platform used as the simulator, the limited workspace is a key issue in designing the MCA. The approach to the input signal within the threshold has linear and non-linear scaling based on the MCA, to replace the value of the input signal with a threshold value for signals that exceed the threshold[7]. Asadi *et al*[8] proposed a non-linear scaling method based on genetic algorithms and optimal MCA to overcome problems pertaining to

select nonlinear scaling parameters based on trial-and-error and inefficient usage of the platform workspace, and to reduce the sensation error between the simulator and aircraft, while satisfying the constraints imposed by the platform boundaries, but it neglects the factor that the motion cueing is significantly different from high and low amplitude signal, and the solution of the Riccati equation is obtained offline for optimal MCA. Luo *et al*[9] and Chen *et al*[10] proposed a variable input, the third-order polynomial method and Hermite function reduction method in combination with classical MCA, respectively. Although the two modification methods have achieved satisfactory results, they are also constrained by the adaptability of the classical MCA filter. The adaptive MCA is concerned, because the classical MCA generated some extra oscillations in some rotational input cases, and this method tries to eliminate the difference of the gravity vector between in the aircraft and in the simulator. It was noted in this study that the difference could not be eliminated since the simulator usually rotates an angle smaller than the aircraft does and the simulator translational acceleration could not be sustained for a long time [11, 12].

In this paper, the nonlinear optimal MCA was adopted and the center of simulator rotation was re-defined. The pilot's head as the center of simulator rotation was chosen to avoid any cross-coupling from simulator rotation to pilot's head translational motion. The method of nonlinear scaling and limiting is adopted to deal with the input signal.

1 Redesign of Nonlinear Optimal MCA

1.1 Pilot Station

The nonlinear optimal MCA input signals are the actual aircraft's longitudinal acceleration and pitch angle velocity. The following is the equations for computing translational accelerations at the pilot station which are implemented in the "Translation to PS (pilot's station)" block.

$$\begin{aligned}
\boldsymbol{a}_{x\mathrm{PS}}^{\mathrm{A}} &= \boldsymbol{a}_{x\mathrm{A}}^{\mathrm{A}} - \boldsymbol{R}_{\mathrm{S}x}(q^2+r^2) + \boldsymbol{R}_{\mathrm{S}y}(pq-\dot{r}) + \boldsymbol{R}_{\mathrm{S}z}(pr-\dot{q}) \\
\boldsymbol{a}_{y\mathrm{PS}}^{\mathrm{A}} &= \boldsymbol{a}_{y\mathrm{A}}^{\mathrm{A}} + \boldsymbol{R}_{\mathrm{S}x}(pq+\dot{r}) - \boldsymbol{R}_{\mathrm{S}y}(p^2+r^2) + \boldsymbol{R}_{\mathrm{S}z}(qr-\dot{p}) \\
\boldsymbol{a}_{y\mathrm{PS}}^{\mathrm{A}} &= \boldsymbol{a}_{z\mathrm{A}}^{\mathrm{A}} + \boldsymbol{R}_{\mathrm{S}x}(pr-\dot{r}) + \boldsymbol{R}_{\mathrm{S}y}(qr+\dot{p}) - \boldsymbol{R}_{\mathrm{S}z}(p^2+q^2)
\end{aligned} \tag{1}$$

where $\boldsymbol{a}_{\mathrm{PS}}^{\mathrm{A}} = [\boldsymbol{a}_{x\mathrm{PS}}^{\mathrm{A}}, \boldsymbol{a}_{y\mathrm{PS}}^{\mathrm{A}}, \boldsymbol{a}_{z\mathrm{PS}}^{\mathrm{A}}]$, $\boldsymbol{a}_{\mathrm{A}}^{\mathrm{A}} = [\boldsymbol{a}_{x\mathrm{A}}^{\mathrm{A}}, \boldsymbol{a}_{y\mathrm{A}}^{\mathrm{A}}, \boldsymbol{a}_{z\mathrm{A}}^{\mathrm{A}}]$, $\boldsymbol{R}_{\mathrm{S}} = [\boldsymbol{R}_{\mathrm{S}x}, \boldsymbol{R}_{\mathrm{S}y}, \boldsymbol{R}_{\mathrm{S}z}]$, $\boldsymbol{\omega}_{\mathrm{A}}^{\mathrm{A}} = [p,q,r]$, $\dot{\boldsymbol{\omega}}_{\mathrm{A}}^{\mathrm{A}} = [\dot{p},\dot{q},\dot{r}]$, $\boldsymbol{a}$ represents the acceleration, x, y, z are the coordinate directions, p, q, r are the attitude angles, A represents the aircraft coordinate, PS represents the pilot's station, and S represents the simulator.

The structure of nonlinear optimal MCA is shown in Fig. 1. The inertial reference frame $\mathrm{Fr_I}$ is earth-fixed with x_I aligned with the gravity vector $\boldsymbol{g}$, and its origin is placed at the center of the fixed platform motion-base. x_I, y_I point forward and the right hand side with respect to the simulator driver. The simulator reference frame

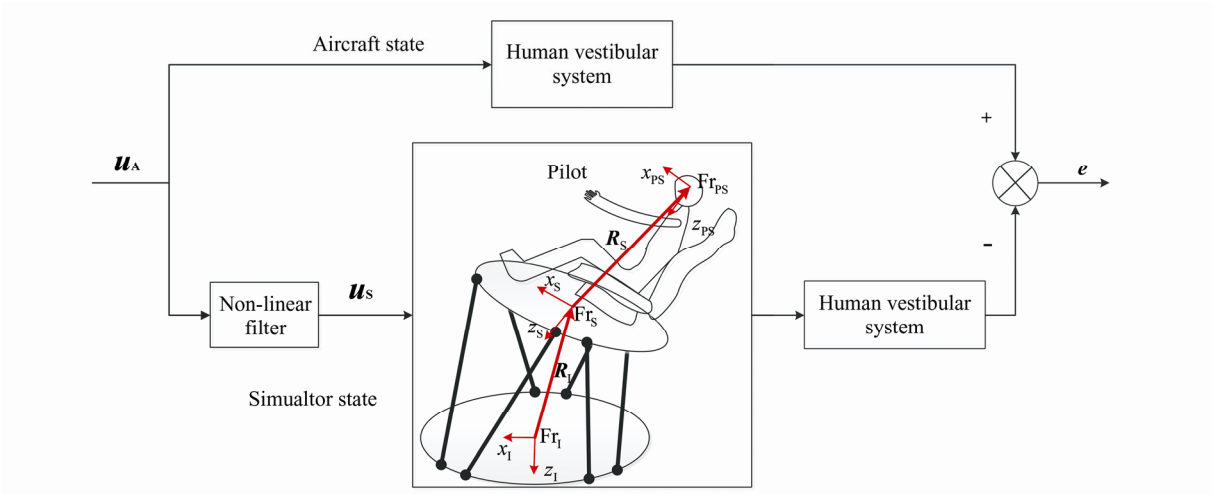

Fig. 1 Nonlinear optimal MCA

$\boldsymbol{u}_\mathrm{A}$: the aircraft input signal; $\boldsymbol{u}_\mathrm{S}$: the simulator motion input signal; $\boldsymbol{e}$: pilot sensation error; $\mathrm{Fr_I}$: the inertial reference frame; $\mathrm{Fr_S}$: the simulator reference frame; $\mathrm{Fr_{PS}}$: the pilot's head reference frame; $\boldsymbol{R}_\mathrm{I}$: radius vector from the inertial reference frame to the simulator reference frame; $\boldsymbol{R}_\mathrm{S}$: radius vector from the simulator reference frame to the pilot's head reference frame; x_I, z_I represent the inertial reference frame coordinate directions; x_S, z_S represent the simulator reference frame coordinate directions; x_PS, z_PS represent the pilot's head reference frame coordinate directions

Fr_S has its origin at the centroid of the simulator payload platform, the centroid of the upper bearing attachment points. The origin is fixed with respect to the simulator payload platform. x_S points forward and z_S points downward with respect to the simulator cockpit, and y_S points toward the pilot's right hand side. The *x*-*y* plane is parallel to the floor of the cockpit. Zaychik[13] proposed modification to the original nonlinear algorithm, which position the PS at the location of the pilot's head. The essence of applying nonlinear washout filters at the PS location as opposed to the centroid of the upper joint bearings of the motion platform is, in fact, the shift of Fr_S from the motion platform to wherever the PS is located. Nonlinear optimal MCA[14,15] can make better use of the motion platform workspace, the design requirements in motion simulation can be solved by adjusting the cost function in the optimization process, and the displacement and acceleration performance of motion platform can be greatly improved by eliminating false cues and presenting a smooth motion perception. However, an inappropriate scaling and limiting in MCA could cause the effect that the motion platform workspace is too conservative, which severely restricts the advantage of the nonlinear optimal MCA. To deal with the problem, Asadi *et al*[16] and Mohammadi *et al*[17] presented the MCA based on model prediction and fuzzy adaptive control. Basically, this MCA includes washout filters and scaling and limiting units, and the scaling and limiting module has a critical impact during motion washout.

1.2 Nonlinear Optimal MCA

The input $\boldsymbol{u}_S$ is given in Eq. (2), $\boldsymbol{a}_x$ is the *x* directions acceleration in the inertial reference frame Fr_I, $\dot{\boldsymbol{\theta}}$ represents pitch angular velocity:

$$\boldsymbol{u}_S=\begin{bmatrix}\dot{\boldsymbol{\theta}}\\ \boldsymbol{a}_x\end{bmatrix}=\begin{bmatrix}\boldsymbol{u}_1\\ \boldsymbol{u}_2\end{bmatrix} \tag{2}$$

The human vestibule system that consists of the semicircular canals and otolith organs can sense translational and rotational movements. The semicircular canals can detect roll, pitch and yaw angular velocity beyond sense threshold. The mathematical model of semicircular canals model is given as:

$$\hat{\dot{\boldsymbol{\theta}}}=\frac{G_{SCC}\,s^2}{s^2+T_1s+T_0}\boldsymbol{u}_1 \tag{3}$$

where $\hat{\dot{\boldsymbol{\theta}}}$ is the sensed angular velocity, *s* is the Laplace variable, T_0, T_1 are described as follows:

$$T_0=\frac{1}{\tau_1\tau_a},\quad T_1=\frac{\tau_1+\tau_a}{\tau_1\tau_a}$$

In addition, τ_1, τ_a are the parameters of the semicircular canals model, G_{SCC} is the angular velocity threshold that scales the response to threshold units.

In an attempt to produce the desired motion cues that most closely represent the perceptual behavior of the aircraft pilot, the confirming case of the integrated perceptual model will be incorporated into the perceptual channel. The visual delay was also neglected since it has only a small effect on the perceptual response. The perceptual input $\boldsymbol{u}=\boldsymbol{u}_S$ for a simulator pilot, and $\boldsymbol{u}=\boldsymbol{u}_A$ for the aircraft pilot. Therefore, $\boldsymbol{u}=\boldsymbol{u}_S-\boldsymbol{u}_A$ can be considered as input to the cueing algorithm. The additional state due to the optokinetic influence must be added to these equations[18]:

$$\hat{\dot{\boldsymbol{\theta}}}_{OK}=\frac{T_2}{s+T_2}(\hat{\dot{\boldsymbol{\theta}}}_A-\hat{\dot{\boldsymbol{\theta}}}_S) \tag{4}$$

where T_2 relates to the time constant.

The semicircular canals state equations become

$$\begin{cases}\dot{\boldsymbol{X}}_{SCC}=\boldsymbol{A}_{SCC}\boldsymbol{X}_{SCC}+\boldsymbol{B}_{SCC}\boldsymbol{u}\\ \dot{\boldsymbol{\theta}}_{PE}=\boldsymbol{C}_{SCC}\boldsymbol{X}_{SCC}+\boldsymbol{D}_{SCC}\boldsymbol{u}\end{cases} \tag{5}$$

where $\boldsymbol{X}_{SCC}$ is the state vector of semicircular canals model, $\dot{\boldsymbol{\theta}}_{PE}$ is the state vector of sensed angular velocity, and $\boldsymbol{A}_{SCC}$, $\boldsymbol{B}_{SCC}$, $\boldsymbol{C}_{SCC}$, and $\boldsymbol{D}_{SCC}$ show the semicircular canals model as one set of state equations.

$$\boldsymbol{A}_{SCC}=\begin{bmatrix}-T_1 & 1 & 0\\ -T_0 & 0 & 0\\ -T_2 & 0 & -T_2\end{bmatrix},\quad \boldsymbol{B}_{SCC}=\begin{bmatrix}-G_{SCC}T_1 & 0\\ -G_{SCC}T_0 & 0\\ -G_{SCC}T_2 & 0\end{bmatrix},$$

$$\boldsymbol{C}_{SCC}=\begin{bmatrix}1 & 0 & 1\end{bmatrix},\quad \boldsymbol{D}_{SCC}=\begin{bmatrix}G_{SCC} & 0\end{bmatrix}$$

The otolith organs can detect lateral, longitudinal and vertical linear acceleration and motion. It transmits information in regard to sense applied specific forces on the human body, responding to linear acceleration or tilting of the head, with consideration of the gravity vector. However, it cannot differentiate translational acceleration from gravity or tilt[19]. The specific force stimulus is

$$\hat{\boldsymbol{f}}_x(s)=G_{OTO}K'_{OTO}\frac{(s+A_0)}{(s+B_0)(s+B_1)}\boldsymbol{f}_x(s) \tag{6}$$

where $\boldsymbol{f}_x(s)$ is the stimulus-specific force, $\hat{\boldsymbol{f}}_x(s)$ is the sensed specific force along the *x*-axis of the head, G_{OTO}, K'_{OTO}, B_0, B_1 and A_0 are the calculated parameters for a static sensitivity, long time constant, short time constant, and lead operator, respectively.

For the center of rotation head-specific force equation is as follows:

$$\boldsymbol{f}_x=\boldsymbol{a}_x+\boldsymbol{g}\theta+\boldsymbol{R}_{Sz}\ddot{\theta} \tag{7}$$

Eq. (7) can be transformed into the Laplace domain:

$$\boldsymbol{f}_x(s)=\boldsymbol{u}_2(s)+(\boldsymbol{g}\frac{1}{s}-\boldsymbol{R}_{Sz}s)\boldsymbol{u}_1(s) \tag{8}$$

The output of the optokinetic influence becomes:

$$\hat{\boldsymbol{f}}_{x\mathrm{OK}}=\frac{T_2}{s+T_2}(\hat{\boldsymbol{f}}_{\mathrm{A}}-\hat{\boldsymbol{f}}_{\mathrm{S}}) \tag{9}$$

The state space representation for the mathematical models of the otolith organs is:

$$\begin{cases}\dot{\boldsymbol{X}}_{\mathrm{OTO}}=\boldsymbol{A}_{\mathrm{OTO}}\boldsymbol{X}_{\mathrm{OTO}}+\boldsymbol{B}_{\mathrm{OTO}}\boldsymbol{u}\\ \hat{\boldsymbol{f}}_{x\mathrm{PE}}=\boldsymbol{C}_{\mathrm{OTO}}\boldsymbol{X}_{\mathrm{OTO}}+\boldsymbol{D}_{\mathrm{OTO}}\boldsymbol{u}\end{cases} \tag{10}$$

where $\boldsymbol{A}_{\mathrm{OTO}}$, $\boldsymbol{B}_{\mathrm{OTO}}$, $\boldsymbol{C}_{\mathrm{OTO}}$, and $\boldsymbol{D}_{\mathrm{OTO}}$ show the otolith models as one set of state equations

$$\boldsymbol{A}_{\mathrm{OTO}}=\begin{bmatrix}0&1&0&0&0&0\\0&-a&1&0&0&0\\0&0&0&0&0&0\\0&0&0&0&1&0\\0&0&0&0&-a&0\\-T_2&0&0&-T_2&0&-T_2\end{bmatrix},$$

$$\boldsymbol{B}_{\mathrm{OTO}}=\begin{bmatrix}c&0\\d-ac&0\\e&0\\0&f\\0&h-af\\T_2G_{\mathrm{OTO}}R_{Sz}&0\end{bmatrix},$$

$$\boldsymbol{C}_{\mathrm{OTO}}=\begin{bmatrix}1&0&0&1&0&1\end{bmatrix},\boldsymbol{D}_{\mathrm{OTO}}=\begin{bmatrix}-G_{\mathrm{OTO}}K'_{\mathrm{OTO}}\boldsymbol{R}_{Sz}&0\end{bmatrix}$$

The representations in Eqs. (5) and (10) can be integrated to arrange a single representation for the human perceptual model:

$$\begin{cases}\dot{\boldsymbol{X}}_{\mathrm{V}}=\boldsymbol{A}_{\mathrm{V}}\boldsymbol{X}_{\mathrm{V}}+\boldsymbol{B}_{\mathrm{V}}\boldsymbol{u}\\ \boldsymbol{y}_{\mathrm{PE}}=\boldsymbol{C}_{\mathrm{V}}\boldsymbol{X}_{\mathrm{V}}+\boldsymbol{D}_{\mathrm{V}}\boldsymbol{u}\end{cases} \tag{11}$$

where $\dot{\boldsymbol{X}}_{\mathrm{V}}$ and $\boldsymbol{y}_{\mathrm{PE}}$ are the combined states vector and the sensed responses, respectively. $\boldsymbol{A}_{\mathrm{V}}$, $\boldsymbol{B}_{\mathrm{V}}$, $\boldsymbol{C}_{\mathrm{V}}$, and $\boldsymbol{D}_{\mathrm{V}}$ represent the vestibular models as one set of state equations:

$$\boldsymbol{A}_{\mathrm{V}}=\begin{bmatrix}\boldsymbol{A}_{\mathrm{SCC}}&\boldsymbol{0}\\\boldsymbol{0}&\boldsymbol{A}_{\mathrm{OTO}}\end{bmatrix},\ \boldsymbol{B}_{\mathrm{V}}=\begin{bmatrix}\boldsymbol{B}_{\mathrm{SCC}}\\\boldsymbol{B}_{\mathrm{OTO}}\end{bmatrix},$$

$$\boldsymbol{C}_{\mathrm{V}}=\begin{bmatrix}\boldsymbol{C}_{\mathrm{SCC}}&\boldsymbol{0}\\\boldsymbol{0}&\boldsymbol{C}_{\mathrm{OTO}}\end{bmatrix},\quad \boldsymbol{D}_{\mathrm{V}}=\begin{bmatrix}\boldsymbol{D}_{\mathrm{SCC}}\\\boldsymbol{D}_{\mathrm{OTO}}\end{bmatrix}$$

The vestibular state error is defined as $\boldsymbol{X}_{\mathrm{e}}$ where $\boldsymbol{X}_{\mathrm{S}}$ and $\boldsymbol{X}_{\mathrm{A}}$ are the vestibular states for simulator and aircraft, respectively. Then the pilot sensation error $\boldsymbol{X}_{\mathrm{e}}=\boldsymbol{X}_{\mathrm{A}}-\boldsymbol{X}_{\mathrm{S}}$ can be calculated in the form:

$$\begin{cases}\dot{\boldsymbol{X}}_{\mathrm{e}}=\boldsymbol{A}_{\mathrm{V}}\boldsymbol{X}_{\mathrm{e}}+\boldsymbol{B}_{\mathrm{V}}\boldsymbol{u}_{\mathrm{S}}-\boldsymbol{B}_{\mathrm{V}}\boldsymbol{u}_{\mathrm{A}}\\ \boldsymbol{e}=\boldsymbol{C}_{\mathrm{V}}\boldsymbol{X}_{\mathrm{e}}+\boldsymbol{D}_{\mathrm{V}}\boldsymbol{u}_{\mathrm{e}}-\boldsymbol{D}_{\mathrm{V}}\boldsymbol{u}_{\mathrm{A}}\end{cases} \tag{12}$$

where $\boldsymbol{u}_{\mathrm{S}}$ and $\boldsymbol{u}_{\mathrm{A}}$ represent the simulator and aircraft input, respectively, as shown in Fig. 1.

The aircraft input $\boldsymbol{u}_{\mathrm{A}}$ consists of filtered noise, and can be represented as:

$$\begin{cases}\dot{\boldsymbol{X}}_{\mathrm{n}}=-\gamma\boldsymbol{X}_{\mathrm{n}}+\gamma\boldsymbol{w}\\ \boldsymbol{u}_{\mathrm{A}}=\boldsymbol{X}_{\mathrm{n}}\end{cases} \tag{13}$$

where $\boldsymbol{X}_n$ is the filtered white noise state, and γ is the break frequency for a given degree of freedom.

By combining Eqs. (11), (12), and (13), we can obtain the desired system equation:

$$\begin{cases}\dot{\boldsymbol{X}}=\boldsymbol{A}\boldsymbol{X}+\boldsymbol{B}\boldsymbol{u}_{\mathrm{S}}+\boldsymbol{H}\boldsymbol{W}\\ \boldsymbol{y}=\begin{bmatrix}\boldsymbol{e}&\boldsymbol{X}_{\mathrm{d}}\end{bmatrix}^{\mathrm{T}}=\boldsymbol{C}\boldsymbol{X}+\boldsymbol{D}\boldsymbol{u}_{\mathrm{S}}\end{cases} \tag{14}$$

where $\boldsymbol{X}=\begin{bmatrix}\boldsymbol{X}_{\mathrm{e}}&\boldsymbol{X}_{\mathrm{d}}&\boldsymbol{X}_{\mathrm{n}}\end{bmatrix}^{\mathrm{T}}$, $\boldsymbol{X}_{\mathrm{d}}$ is motion platform states, $\boldsymbol{y}$ is the desired output, and $\boldsymbol{A}=\begin{bmatrix}\boldsymbol{A}_{\mathrm{V}}&\boldsymbol{0}&-\boldsymbol{B}_{\mathrm{V}}\\\boldsymbol{0}&\boldsymbol{A}_{\mathrm{d}}&\boldsymbol{0}\\\boldsymbol{0}&\boldsymbol{0}&-\gamma\end{bmatrix}$,

$\boldsymbol{B}=\begin{bmatrix}\boldsymbol{B}_{\mathrm{V}}\\\boldsymbol{B}_{\mathrm{d}}\\\boldsymbol{0}\end{bmatrix}$, $\boldsymbol{H}=\begin{bmatrix}\boldsymbol{0}\\\boldsymbol{0}\\\gamma\end{bmatrix}$, $\boldsymbol{C}=\begin{bmatrix}\boldsymbol{C}_{\mathrm{V}}&\boldsymbol{0}&-\boldsymbol{D}_{\mathrm{V}}\\\boldsymbol{0}&\boldsymbol{I}&\boldsymbol{0}\end{bmatrix}$,

$\boldsymbol{D}=\begin{bmatrix}\boldsymbol{D}_{\mathrm{V}}\\\boldsymbol{0}\end{bmatrix}$, $\boldsymbol{A}_{\mathrm{d}}=\begin{bmatrix}0&1\\0&0\end{bmatrix}$, $\boldsymbol{B}_{\mathrm{d}}=\begin{bmatrix}0\\1\end{bmatrix}$.

The cost function is augmented with an additional term $\mathrm{e}^{2\alpha t}$ proposed by Anderson.

$$\begin{cases}\dot{\boldsymbol{X}}=(\boldsymbol{A}'+\alpha\boldsymbol{I})\boldsymbol{X}+\boldsymbol{B}\boldsymbol{u}'+\boldsymbol{H}\boldsymbol{W}\\ J'=E\left\{\int_{t_0}^{t_1}\mathrm{e}^{2\alpha t}(\boldsymbol{X}^{\mathrm{T}}\boldsymbol{R}'_1\boldsymbol{X}+\boldsymbol{u}'^{\mathrm{T}}\boldsymbol{R}_2\boldsymbol{u}')\mathrm{d}t\right\}\end{cases} \tag{15}$$

where $\boldsymbol{u}'=\boldsymbol{u}_{\mathrm{S}}+\boldsymbol{R}_2^{-1}\boldsymbol{R}_{12}^{\mathrm{T}}\boldsymbol{X}$, $\boldsymbol{R}'_1=\boldsymbol{R}_1-\boldsymbol{R}_{12}\boldsymbol{R}_2^{-1}\boldsymbol{R}_{12}^{\mathrm{T}}$, $\boldsymbol{R}_1=\boldsymbol{C}^{\mathrm{T}}\boldsymbol{G}\boldsymbol{C}$, $\boldsymbol{R}_{12}=\boldsymbol{C}^{\mathrm{T}}\boldsymbol{G}\boldsymbol{D}$, $\boldsymbol{R}_2=\boldsymbol{R}+\boldsymbol{D}^{\mathrm{T}}\boldsymbol{G}\boldsymbol{D}$, $\boldsymbol{G}=\mathrm{diag}[\boldsymbol{Q},\boldsymbol{R}_{\mathrm{d}}]$.

When $\boldsymbol{u}'=-\boldsymbol{R}_2^{-1}\boldsymbol{R}^{\mathrm{T}}\boldsymbol{P}(\alpha)\boldsymbol{X}$, the cost function is minimized, where $\boldsymbol{P}(\alpha)$ is the solution of the algebraic Riccati equation

$$\begin{aligned}&\boldsymbol{R}'_1-\boldsymbol{P}(\alpha)\boldsymbol{B}\boldsymbol{R}_2^{-1}\boldsymbol{B}^{\mathrm{T}}\boldsymbol{P}(\alpha)+(\boldsymbol{A}'+\alpha\boldsymbol{I})^{\mathrm{T}}\boldsymbol{P}(\alpha)\\&\quad+\boldsymbol{P}(\alpha)(\boldsymbol{A}'+\alpha\boldsymbol{I})=0\end{aligned} \tag{16}$$

Eq. (16) can be substituted into Eq. (15) by solving for $\boldsymbol{u}_{\mathrm{S}}$

$$\boldsymbol{u}_{\mathrm{S}}=-[\boldsymbol{R}_2^{-1}(\boldsymbol{B}^{\mathrm{T}}\boldsymbol{P}(\alpha)+\boldsymbol{R}_{12}^{\mathrm{T}})]\boldsymbol{X} \tag{17}$$

By defining a matrix $\boldsymbol{K}$, $\boldsymbol{u}_{\mathrm{S}}=-\boldsymbol{K}(\alpha)\boldsymbol{X}\Rightarrow$

$\boldsymbol{K}(\alpha)=\boldsymbol{R}_2^{-1}(\boldsymbol{B}^{\mathrm{T}}\boldsymbol{P}(\alpha)+\boldsymbol{R}_{12})$, $\boldsymbol{X}=[\boldsymbol{X}_{\mathrm{e}}\quad \boldsymbol{X}_{\mathrm{d}}\quad \boldsymbol{X}_{\mathrm{n}}]^{\mathrm{T}}$, we can obtain:

$$\boldsymbol{u}_{\mathrm{S}}=-\begin{bmatrix}\boldsymbol{K}_1(\alpha) & \boldsymbol{K}_2(\alpha)\end{bmatrix}\begin{bmatrix}\boldsymbol{X}_{\mathrm{e}}\\ \boldsymbol{X}_{\mathrm{d}}\end{bmatrix}-\boldsymbol{K}_3(\alpha)\boldsymbol{u}_{\mathrm{A}} \tag{18}$$

and the Riccati equation solution $\boldsymbol{P}(\alpha)$ can be partitioned as

$$\boldsymbol{P}(\alpha)=\begin{bmatrix}\boldsymbol{P}_{11}(\alpha) & \boldsymbol{P}_{12}(\alpha) & \boldsymbol{P}_{13}(\alpha)\\ \boldsymbol{P}_{21}(\alpha) & \boldsymbol{P}_{22}(\alpha) & \boldsymbol{P}_{23}(\alpha)\\ \boldsymbol{P}_{31}(\alpha) & \boldsymbol{P}_{32}(\alpha) & \boldsymbol{P}_{33}(\alpha)\end{bmatrix} \tag{19}$$

$\boldsymbol{K}$ is given in Eq. (18) and results in

$$\begin{aligned}\boldsymbol{K}_1(\alpha)&=\boldsymbol{R}_2^{-1}[\boldsymbol{B}_{\mathrm{V}}^{\mathrm{T}}\boldsymbol{P}_{11}+\boldsymbol{B}_{\mathrm{d}}^{\mathrm{T}}\boldsymbol{P}_{21}+\boldsymbol{D}_{\mathrm{V}}^{\mathrm{T}}\boldsymbol{Q}\boldsymbol{C}_{\mathrm{V}}]\\ \boldsymbol{K}_2(\alpha)&=\boldsymbol{R}_2^{-1}[\boldsymbol{B}_{\mathrm{V}}^{\mathrm{T}}\boldsymbol{P}_{12}+\boldsymbol{B}_{\mathrm{d}}^{\mathrm{T}}\boldsymbol{P}_{22}]\\ \boldsymbol{K}_3(\alpha)&=\boldsymbol{R}_2^{-1}[\boldsymbol{B}_{\mathrm{V}}^{\mathrm{T}}\boldsymbol{P}_{11}+\boldsymbol{B}_{\mathrm{d}}^{\mathrm{T}}\boldsymbol{P}_{23}-\boldsymbol{D}_{\mathrm{V}}^{\mathrm{T}}\boldsymbol{Q}\boldsymbol{C}_{\mathrm{V}}]\end{aligned} \tag{20}$$

where, by symmetry, $\boldsymbol{P}_{12}=\boldsymbol{P}_{21}{}^{\mathrm{T}}$.

As $\boldsymbol{u}_{\mathrm{A}}=\boldsymbol{X}_{\mathrm{n}}$, the state corresponding to $\boldsymbol{X}_{\mathrm{n}}$ is removed from

$$\begin{bmatrix}\dot{\boldsymbol{X}}_{\mathrm{e}}\\ \dot{\boldsymbol{X}}_{\mathrm{d}}\end{bmatrix}=\begin{bmatrix}\boldsymbol{A}_{\mathrm{V}} & \boldsymbol{0} & -\boldsymbol{B}_{\mathrm{V}}\\ \boldsymbol{0} & \boldsymbol{A}_{\mathrm{d}} & \boldsymbol{0}\end{bmatrix}\begin{bmatrix}\boldsymbol{X}_{\mathrm{e}}\\ \boldsymbol{X}_{\mathrm{d}}\\ \boldsymbol{u}_{\mathrm{A}}\end{bmatrix}+\begin{bmatrix}\boldsymbol{B}_{\mathrm{V}}\\ \boldsymbol{B}_{\mathrm{d}}\end{bmatrix}\boldsymbol{u}_{\mathrm{S}} \tag{21}$$

Substitution of (20) into (21)

$$\begin{aligned}\begin{bmatrix}\dot{\boldsymbol{X}}_{\mathrm{e}}\\ \dot{\boldsymbol{X}}_{\mathrm{d}}\end{bmatrix}&=\begin{bmatrix}\boldsymbol{A}_{\mathrm{V}}-\boldsymbol{B}_{\mathrm{V}}\boldsymbol{K}_1(\alpha) & -\boldsymbol{B}_{\mathrm{V}}\boldsymbol{K}_2(\alpha)\\ -\boldsymbol{B}_{\mathrm{d}}\boldsymbol{K}_1(\alpha) & \boldsymbol{A}_{\mathrm{d}}-\boldsymbol{B}_{\mathrm{d}}\boldsymbol{K}_2(\alpha)\end{bmatrix}\begin{bmatrix}\boldsymbol{X}_{\mathrm{e}}\\ \boldsymbol{X}_{\mathrm{d}}\end{bmatrix}\\ &+\begin{bmatrix}-\boldsymbol{B}_{\mathrm{V}}(\boldsymbol{I}+\boldsymbol{K}_3(\alpha))\\ -\boldsymbol{B}_{\mathrm{d}}\boldsymbol{K}_3(\alpha)\end{bmatrix}\boldsymbol{u}_{\mathrm{A}}\end{aligned} \tag{22}$$

A nonlinear control law is chosen to make α dependent upon the system states:

$$\alpha=\boldsymbol{X}_{\mathrm{d}}^{\mathrm{T}}\boldsymbol{Q}_2\boldsymbol{X}_{\mathrm{d}} \tag{23}$$

where $\boldsymbol{Q}_2$ is a weighting matrix that is at least positive semi-definite. The feedback matrix $\boldsymbol{K}(\alpha)$ is then determined by solving the Riccati equation of Eq. (15) in real time as a function of α.

1.3 Nonlinear Scaling and Limiting

In the structure of the washout algorithm, no matter how classical, adaptive or optimal the MCA, they all have a scaling and limiting module to ensure that the washout signal conforms to the characteristics of the simulated actual movement, and the driver can drive a real aircraft in the simulator. Usually, there are two types: linear and nonlinear[20], such as third-order polynomial method, equal scaling and limiting method. The common problem pertaining to the scaling and limiting module is their tuning process, which is based on trial-and-error. This is a sub-optimal process that affects the generated motions, makes the simulator motion conservative, and produces false motion cues. For instance, the third-order polynomial method that Telban proposed[7] does not limit the local extreme point. When input signal monotonously increases or decreases within a large amplitude range, it is easy to cause the result that output signal fall into the local extreme value and lead to signal distortion[10]. This paper proposes a scaling & limiting strategy to deal with input signal, and the formula is shown in Eq. (24),

$$y_{\mathrm{tran}}=\begin{cases}k_{\mathrm{l}}\times y_{\mathrm{in}}, & |y_{\mathrm{in}}|<y_{\mathrm{l}}\\ y_{\mathrm{in}}, & |y_{\mathrm{in}}|<y_{\mathrm{u}}\\ k_{\mathrm{u}}\times(y_{\mathrm{in}}-y_{\mathrm{u}})+y_{\mathrm{u}}, & |y_{\mathrm{in}}|>y_{\mathrm{u}}\end{cases} \tag{24}$$

where y_{in}, y_{l}, y_{u} are the input signal, lower and upper scaling boundary, respectively. k_{l}, k_{u} are the motion perception boundary parameters. The general selection range should be between 1-2 for the lower motion perception scaling boundary factor k_{l}. The most appropriate upper motion perception scaling boundary factor k_{u} for most commercial simulators is chosen empirically as 0.5 in both the translational and rotational motion channels[21]. y_{tran} is the transformed input acceleration, and it is limited within the maximum acceleration range of the motion platform to protect the safety of motion simulation.

2 Simulation Analysis

In this paper, in order to verify the reliability of the method, nonlinear optimal MCA is adopted in the longitudinal and pitch directions, and its structure is shown in Fig. 2.

Pilot's station vector $\boldsymbol{R}_{\mathrm{S}}$=[0.01, 0.25, 1.75] in meters. Longitudinal acceleration is shown in Fig. 3. In order to observe the influence of the coordinated tilt acceleration, the pitch angular velocity is set as zero in the pitch direction. The solid line represents the actual input acceleration, and the dotted line represents the acceleration after non-linear scaling and limiting. The nonlinear scaling and limiting acceleration is determined by Eq. (24), and y_{l}, y_{u} are 1 m/s^2, 3 m/s^2, the parameter k_{l}, k_{u} are 1.35, 0.5, respectively. The original signal is as large as possible in the range of the low amplitude, so that the driver can feel the movement in advance. To ensure the fidelity of simulation acceleration, the original signal is maintained in the range of the medium amplitude. Especially, the scaling and limiting should be paid attention in the range of the high amplitude. The appropriate parameter can not only prevent the movement platform from exceeding the limit of the workspace, but also ensure the movement characteristics of the washout signal.

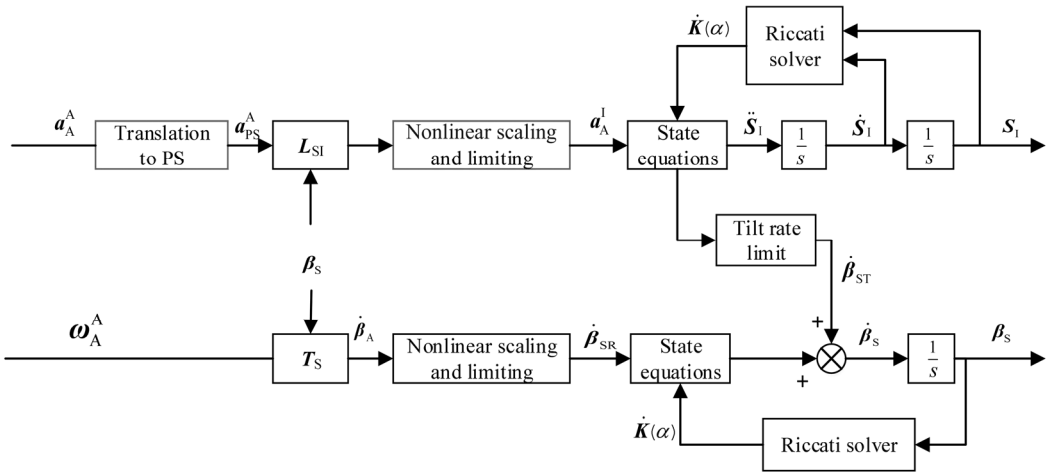

Fig. 2 Longitudinal and pitch nonlinear optimal MCA

a_A^A : aircraft acceleration; a_{PS}^A : pilot's head vestibule acceleration in simulator; a_A^I : acceleration after nonlinear scaling & limiting; PS: pilot station; L_{SI}: transformation matrix from simulator into inertial frame; T_S: transformation matrix from angular velocity to Euler angle rates; $\dot{\beta}_A$: angular velocity after T_S; $\dot{\beta}_{SR}$: angular velocity after nonlinear scaling & limiting; $\dot{\beta}_{ST}$: washout angular velocity after tilt rate limit; $\dot{\beta}_S$: the sum of washout angular velocity; β_S : washout angular displacement; s: Laplace variable; $\ddot{S}_I$: washout acceleration in the inertial frame; $\dot{S}_I$: washout velocity in the inertial frame; S_I : washout displacement in the inertial frame; $K(\alpha)$: the feedback matrix

Pilot's station vector R_S=[0.01, 0.25, 1.75] in meters. Longitudinal acceleration is shown in Fig. 3. In order to observe the influence of the coordinated tilt acceleration, the pitch angular velocity is set as zero in the pitch direction. The solid line represents the actual Input acceleration, and the dotted line represents the acceleration after non-linear scaling and limiting. The nonlinear scaling and limiting acceleration is determined by Eq. (24), and y_l, y_u are 1 m/s^2, 3 m/s^2, the parameter k_l, k_u are 1.35, 0.5, respectively. The original signal is as large as possible in the range of the low amplitude, so that the driver can feel the movement in advance. To ensure the fidelity of simulation acceleration, the original signal is maintained in the range of the medium amplitude. Especially, the scaling and limiting should be paid attention in the range of the high amplitude. The appropriate parameter can not only prevent the movement platform from exceeding the limit of the workspace, but also ensure the movement characteristics of the washout signal.

Figure 4 shows the sense acceleration of the longitudinal direction after the nonlinear optimal MCA, nonlinear scaling and limiting. The chain line is the pilot's perceived acceleration in the aircraft, which is the actual perceived acceleration. The dotted line is the washout sensory acceleration by the improved nonlinear optimal MCA. The solid line is the unimproved nonlinear optimal MCA. That is, the driver's sensory center is in the center of the motion platform, and the scaling and

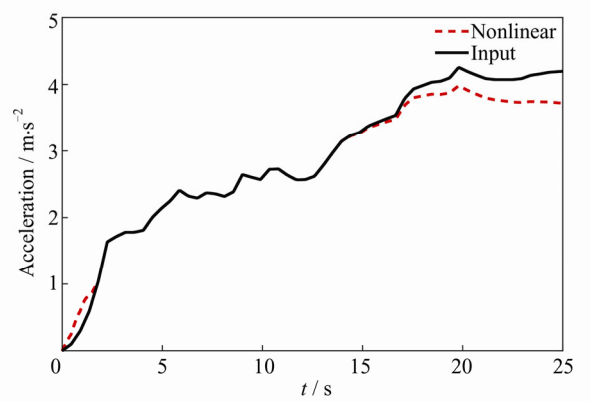

Fig. 3 Longitudinal acceleration signal

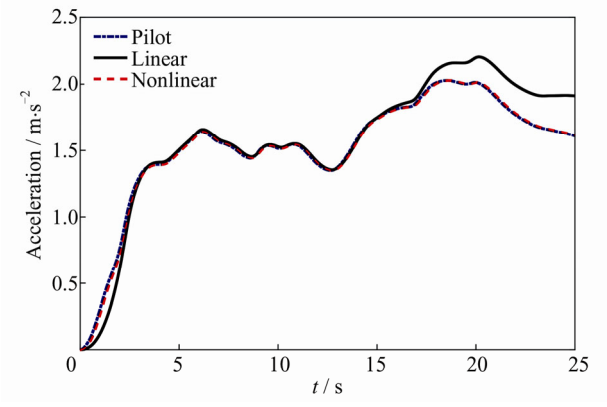

Fig. 4 Sense acceleration

limiting module is linear scaling. The washout acceleration is evaluated by the human vestibular model, then the sense acceleration is obtained. Therefore, it can be seen that the improved washout algorithm is closer to the actual movement sense as a whole, while the nonlinear optimal MCA with linear scaling and limiting has certain errors in the range of the low- and high-amplitude.

The washout displacement of the algorithm is shown in Fig. 5 under linear and nonlinear conditions. On the whole, the longitudinal washout displacement of nonlinear method for motion platform is upper than the linear in the range of 0-1.5 s, and the maximum washout displacement does not exceed the linear method. It indicates that the improved method has the higher feedback speed in the motion simulation performance, and the safety of workspace is guaranteed. About at 2.5 s, they all reach the maximum washout displacement of the motion platform. The maximum washout displacement of the linear method is 0.38 m, and the nonlinear method is 0.36 m, so the improved method is more capable of using a smaller motion space to achieve the same motion simulation, to ensure the safety of motion platform. In the final stage of the motion simulation, the motion platform can be restored to the neutral position more quickly so that the sufficient time and workspace can be provided for the next movement.

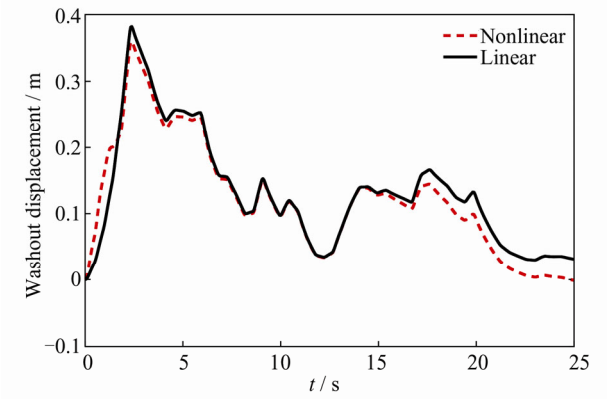

Fig. 5 Washout displacement of the algorithm under linear and nonlinear conditions

As shown in Fig. 6, both linear and nonlinear methods represent the washout sensory angular velocity. The two horizontal lines are the upper and lower thresholds of the semicircular canal±0.062 8 rad/s. The core of the MCA is to use the principle of tilt coordination to simulate continuous acceleration, but it cannot exceed the semicircular canal threshold, otherwise the washout process will inevitably be perceived for the occurrence of tilt coordination. To avoid this as much as possible during the motion simulation process, in the conventional processing measure, the angular velocity limiter is added into tilt coordination channel to ensure tilt angular velocity within the semicircular canal threshold. Although this method can avoid the occurrence of false cue, it will simultaneously lead to the filter of the angular velocity signal beyond the semicircular canal threshold. The part of the simulation continuous acceleration cannot be duplicated beyond the semicircular canal threshold. Therefore, the nonlinear control strategy is adopted to ensure the washout sense angular velocity within the threshold. Finally, the sense angular velocity tends to zero, which can be used for the next movement and provide adequate time preparation.

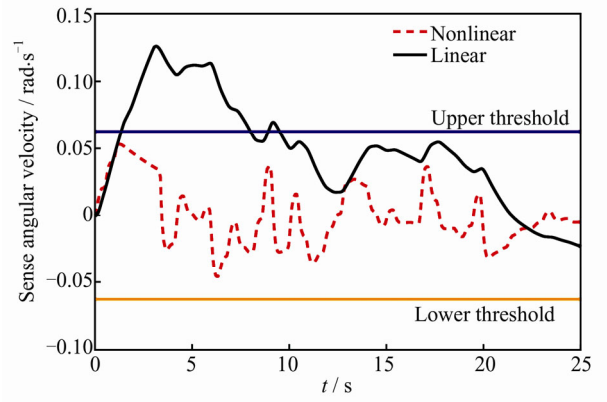

Fig. 6 Sense angular velocity

3 Conclusion

The MCA has responsibility for duplicating the actual flight status, but the aircraft motions can be transformed into the simulator motions within the motion platform's physical limitations. In designing the MCA, the scaling and limiting units play a major role in keeping the motions with the physical constraints of the simulator. The scaling and limiting module should be used along with washout filters to reduce the magnitude of the translational and rotational motion signals uniformly across all frequencies for all kinds of MCA, so as to decrease the effects due to workspace limitations in reproducing the simulator motions, and enhancing realism of motion sensation. In this article, by establishing a mathematical model of the nonlinear optimal MCA, PS is considered, the control strategy of nonlinear scaling and limiting is designed. The simulation results indicate that the proposed method is able to accurately duplicate motions in a simu-

lator platform. The washout displacement and sense angular velocity signal are in conformity with shape-following criteria. And the proposed method can reduce the sensation error of motion washout process with higher fidelity and higher efficiency in platform usage without violating the physical limitations of the simulator, to eliminate the false cues occurrence. Nevertheless, there are still shortcomings to overcome, such as, how the scaling factor further improve the adaptability in the nonlinear scaling module? How can the scaling boundary division impact on the motion perception in the MCA? The researchers will have an interest in future research.

References

[1] Conrad B, Schmidt S F. Motion Drive Signals for Piloted Flight Simulators [EB/OL]. [2021-08-15]. *https://ntrs.nasa.gov/archive/ nasa/casi.ntrs.nasa.gov/*19700017803*.pdf*.

[2] Nehaoua L, Amouri A, Arioui H. Classic and adaptive washout comparison for a low cost driving simulator [C]// *Proceedings of the* 20*th IEEE International Symposium on Intelligent Control and the* 13*th Mediterranean Conference on Control and Automation*. Piscataway: IEEE, 2005: 586- 591.

[3] Asadi H, Mohammadi A, Mohamed S, *et al*. A particle swarm optimization-based washout filter for improving simulator motion fidelity [C]// *Proceedings of the* 2016 *IEEE International Conference on Systems*, *Man*, *and Cybernetics* (*SMC*). New York: IEEE, 2016: 1963-1968.

[4] Bowles R L, Parrish R V, Dieudonne J E. Coordinated adaptive washout for motion simulators [J]. *Journal of Aircraft*, 1975, **12**(1): 44-50.

[5] Sivan R, Ish-Shalom J, Huang J K. An optimal control approach to the design of moving flight simulators [J]. *IEEE Transactions on Systems*, *Man and Cybernetics*, 1982, **12**(6): 818-827.

[6] Reid L D, Nahon M A. Flight Simulation Motion-base Drive Algorithms: Part 1—Developing and Testing the Equations [EB/OL]. [2021-08-15]. *http://repository.tudelft.nl/assets/uuid*:45b071*c*0-0568-4*e*8*f*-948*f-dfa*52*d*350665/296*.pdf*.

[7] Telban R, Wu W, Cardullo F M. Motion cuing algorithm development: Initial investigation and redesign of the algorithms [EB/OL]. [2021-08-15]. *https://ntrs.nasa.gov/archive/nasa/casi.ntrs.nasa.gov/*20000041705*.pdf*.

[8] Asadi H, Chee P L. A genetic algorithm-based nonlinear scaling method for optimal MCA in driving simulator [J]. *Proc IMechE Part I*: *Journal of Systems and Control Engineering*, 2018, **232**(8): 1025-1038.

[9] Luo Z H, Wei Y D, Zhou X J. Research on variable input MCA for Stewart platform vehicle simulator [J]. *Journal of Zhejiang University* (*Engineering Science*), 2013, **47**(2): 238-243(Ch).

[10] Chen W, Jiang G H, Chao J G. Signal scaling strategies for motion-base spaceflight simulators [J]. *Journal of Beijing University of Aeronautics and Astronautics*, 2012, **38**(3): 324-329.

[11] Wu W. *Development of Cueing Algorithm for the Control of Simulator Motion Systems* [D]. New York: Binghamton University, 1997.

[12] Wu W, Cardullo F. Is there an optimum motion cueing algorithm? [C]//*AIAA Modeling and Simulation Technologies Conference*. Reston: AIAA, 1997: 3506.

[13] Zaychik K B, Cardullo F M. Nonlinear Motion Cueing Algorithm: Filtering at Pilot Station and Development of the Nonlinear Optimal Filters for Pitch and Roll [EB/OL]. [2021-08-06]. *https*://*ntrs.nasa.gov/citations/*20120008933*.pdf*.

[14] Telban R J, Cardullo F M, Houck J A. A nonlinear, human-centered approach to motion cueing with a neurocomputing solver [C]// *AIAA Modeling and Simulation Technologies Conference and Exhibit*. Reston: AIAA, 2002: 4692.

[15] Pahlevaninezhad M, Das P, Drobnik J, *et al*. A nonlinear optimal control approach based on the control-Lyapunov function for an AC/DC converter used in electric aircrafts [J]. *IEEE Transactions on Industrial Informatics*, 2012, **8**(3): 596-614.

[16] Asadi H, Mohamed S, Nahavandi S. Incorporating human perception with the motion washout filter using fuzzy logic control [J]. *IEEE*/*ASME Transactions on Mechatronics*, 2015, **20**(6): 3276-3284.

[17] Mohammadi A, Asadi H, Mohamed S, *et al*. Optimizing model predictive control horizons using genetic algorithm for motion cueing algorithm [J]. *Expert Systems with Applications*, 2018, **92**: 73-81.

[18] Telban R J, Cardullo F M. MCA development: Human centered linear and nonlinear approaches [EB/OL]. [2021-09-06]. *https://ntrs.nasa.gov/citations/*20050180246*.pdf*.

[19] Hosman R, van der Vaart J C. *Vestibular Models and Thresholds of Motion Perception*: *Results of Tests in a Flight Simulator* [R]. Delft: Delft University of Technology, 1978.

[20] Zhu D Y, Duan S L, Shang J Q, *et al*. A novel nonlinear scaling method for optimal motion cueing algorithm in flight simulator [J]. *Wuhan University Journal of Natural Sciences*, 2020, **25**(5): 452-460.

[21] Nahon M A, Reid L D. Simulator motion-drive algorithms—A designer's perspective [J]. *J Guid ContrDynam*, 1990, **13**(2): 356-362.

□